Biogeochemical Cycling of Silver in Acidic, Weathering Environments

Jeremiah Shuster [1,2,*] [iD]**, Frank Reith [1,2], Matthew R. M. Izawa [3], Roberta L. Flemming [4], Neil R. Banerjee [4] and Gordon Southam [5]**

[1] School of Biological Sciences, The University of Adelaide, Adelaide, SA 5005, Australia; Frank.Reith@CSIRO.au
[2] CSIRO Land and Water, Contaminant Chemistry and Ecotoxicology, PMB2, Glen Osmond, SA 5064, Australia
[3] Institute for Study of the Earth's Interior, Okayama University, Okayama, Okayama Prefecture 700-0082, Japan; matthew_izawa@okayama-u.ac.jp
[4] Department of Earth Science, The University of Western Ontario, London, ON N6A 3K7, Canada; rflemmin@uwo.ca (R.L.F.); nbanerj3@uwo.ca (N.R.B.)
[5] School of Earth & Environmental Sciences, The University of Queensland, St. Lucia, QLD 4218, Australia; g.southam@uq.edu.au
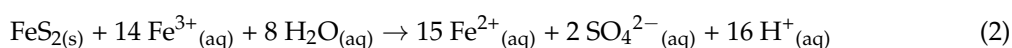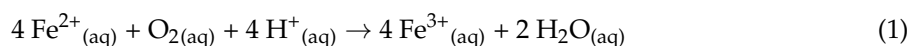* Correspondence: jeremiah.shuster@adelaide.edu.au; Tel.: +61-8-8313-5352

Abstract: Under acidic, weathering conditions, silver (Ag) is considered to be highly mobile and can be dispersed within near-surface environments. In this study, a range of regolith materials were sampled from three abandoned open pit mines located in the Iberian Pyrite Belt, Spain. Samples were analyzed for Ag mineralogy, content, and distribution using micro-analytical techniques and high-resolution electron microscopy. While Ag concentrations were variable within these materials, elevated Ag concentrations occurred in gossans. The detection of Ag within younger regolith materials, i.e., terrace iron formations and mine soils, indicated that Ag cycling was a continuous process. Microbial microfossils were observed within crevices of gossan and their presence highlights the preservation of mineralized cells and the potential for biogeochemical processes contributing to metal mobility in the rock record. An acidophilic, iron-oxidizing microbial consortium was enriched from terrace iron formations. When the microbial consortium was exposed to dissolved Ag, more than 90% of Ag precipitated out of solution as argentojarosite. In terms of biogeochemical Ag cycling, this demonstrates that Ag re-precipitation processes may occur rapidly in comparison to Ag dissolution processes. The kinetics of Ag mobility was estimated for each type of regolith material. Gossans represented 0.6–146.7 years of biogeochemical Ag cycling while terrace iron formation and mine soils represented 1.9–42.7 years and 0.7–1.6 years of Ag biogeochemical cycling, respectively. Biogeochemical processes were interpreted from the chemical and structural characterization of regolith material and demonstrated that Ag can be highly dispersed throughout an acidic, weathering environment.

Keywords: silver biogeochemical cycling; argentojarosite; iron-oxidizing bacteria/archaea; gossan; terrace iron formations

---

1. Introduction

Silver commonly occurs as Ag-bearing sulfides and (Hg/Au)-Ag-alloys in primary metal sulfide deposits [1,2]. While metal sulfide oxidation is mechanistically an abiotic reaction [3–7], acidophilic, iron-/sulfur-oxidizing bacteria/archaea are known to catalyze the rate of these reactions up to seven orders of magnitude [8–11]. As a result, biogeochemical weathering of a gold-bearing

polymetallic sulfide ore can lead to the liberation of Au–Ag grains [12]. Furthermore, the preferential thiosulfate-leaching of Ag has been suggested as a mechanism for gold enrichment of gold grains and nuggets [13–16]. Therefore, the movement of Ag under near-surface weathering conditions is enhanced through dissolution and re-precipitation processes [17,18]. Silver is considered to be a highly mobile metal because it can be transported within hydrological regimes as a dissolved Ag^+ ion or as a compound when complexed with Cl^-, SO_4^{2-} or NO_3^- ligands. Like secondary Au, elemental Ag can also be transported as nanoparticles; furthermore, Ag^+ can be incorporated into a variety of secondary minerals [1,13,19,20]. During (bio)oxidation of iron sulfides, acidophilic, iron-oxidizing bacteria such as *Acidithiobacillus ferrooxidans* produce dissolved Fe^{3+}, H^+ and SO_4^{2-} as by-products of their active metabolism (Reactions (1) and (2)) [21,22]. Jarosite-group minerals have the general formula of $AG_3(TO_4)_2(OH)_6$ where the *G* and *T* sites contain Fe^{3+} and SO_4^{2-}, respectively. The *A* site often contains common monovalent cations such as K^+, Na^+ and H_3O^- which can be substituted by Pb^{2+}, NH_4^+ or Ag^+. The occurrence of argentojarosite ($AgFe_3(SO_4)_2(OH)_6$) is rare relative to other jarosite-group endmembers; however, it accounts for a substantial fraction of Ag within gossan and is thought to reflect the early phases of gossanization [23,24]. Under acidic weathering conditions, such as those occurring within and around open pit mine sites, dissolved Fe^{3+}, H^+ and SO_4^{2-} can form jarosite-group minerals that could act as a "sink" for Ag^+ [25–30].

$$4\ Fe^{2+}_{(aq)} + O_{2(aq)} + 4\ H^+_{(aq)} \rightarrow 4\ Fe^{3+}_{(aq)} + 2\ H_2O_{(aq)} \tag{1}$$

$$FeS_{2(s)} + 14\ Fe^{3+}_{(aq)} + 8\ H_2O_{(aq)} \rightarrow 15\ Fe^{2+}_{(aq)} + 2\ SO_4^{2-}_{(aq)} + 16\ H^+_{(aq)} \tag{2}$$

From a biogeochemical perspective, the dissolution and subsequent re-precipitation of gold has been the focus of many studies regarding precious metal mobility within weathering environments since its cycling is closely linked to iron and sulfur cycles [31,32]. However, in contemporaneous to gold biogeochemical cycling, little is known about the "fate" of Ag in regard to its kinetic mobility within an acidic weathering environment. Therefore, the primary purpose of this study was to estimate the extent of Ag biogeochemical cycling within regolith materials from an acidic, weathering environment. In doing so, gossan was characterized to identify structures that could be relicts of "past" biogeochemical processes. Furthermore, the effect of an acidophilic, iron-oxidizing microbial consortium on the stability of soluble Ag was also determined. This study highlights the characterization of natural materials as an important means for interpreting biogeochemical processes in the rock record and how these processes contributed to the mobility of Ag within an acidic weathering environment.

2. Materials and Methods

2.1. Study Sites and Sample Acquisition

The Iberian Pyrite Belt (IPB) is located in southwestern Spain and Portugal and is the largest ore province in the Earth's crust, containing many massive sulfide deposits [33–37]. At the surface, these ore bodies are highly oxidized and often contain a ferric iron-rich cap, i.e., gossan. These caps can range from meters to tens of meters in thickness and are known to contain elevated concentrations of gold and silver that were exploited during Roman times. More recently in mining history, gossans were used as indicators for targeting the primary ore bodies below the surface [37–41]. The San Telmo, San Miguel and Tharsis mines (near Huelva, Spain) once held important economic metals reserves including Ag and Au (Figure 1A) [42]. Mining activity has displaced large quantities of earth and these sites continue to be subjected to physical and biogeochemical weathering. These weathering processes, influenced by seasonal variations in precipitation, contribute to further weathering of gossans and formation of younger regolith materials including terrace iron formations and mine surface soils [43]. These regolith materials commonly occur in open-pit mines and represent different types of materials in which Ag biogeochemical cycling can occur. Therefore, these mines are model

weathering environments containing regolith materials ideal for estimating the kinetics mobility and dispersion of Ag under acidic conditions. For this study, gossans, terrace iron formations and mine soils were collected from San Telmo, San Miguel and Tharsis mines, Spain. Samples of weathered gossans were obtained from debris piles located proximal to remnants of the cap. Terrace iron formations were sampled aseptically from water runoffs on the bench faces or from drainage channels. The average pH of these flowing waters was 3.9 ($\pm$0.1 pH unit) determined using ColorpHast™ pH indicator strips. Mine soils, containing soluble salts, were sampled from the surface of road workings (Figure 1B–E).
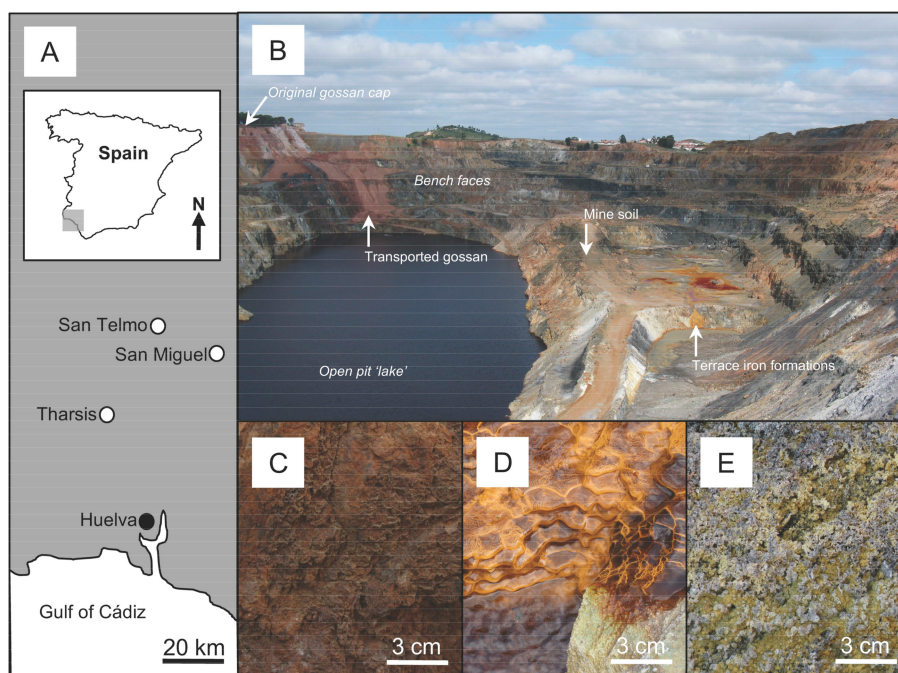

Figure 1. A map of southern Spain and locations of the abandoned San Telmo, San Miguel and Tharsis open pit mines (**A**); a schematic photograph of an open pit mine illustrating the occurrences of regolith materials and regions from which representative samples were obtained (**B**); representative photographs of transported gossan (**C**); terrace iron formation (**D**); and mine soils (**E**).

2.2. Chemical and Structural Characterization of Regolith Materials

Aliquots of gossans, terrace iron formations and mine soils were powdered to a particle size less than 5 µm for X-ray Diffraction (XRD) analysis. Data were collected from 2 to 82° 2θ with a step size of 0.02° and scanning speed of 10°/min using a Rigaku Rotaflex diffractometer (Rigaku, Tokyo, Japan) operating at 45 kV and 160 mA with a high brightness cobalt rotating anode source (Co Kα, λ = 1.7902 Å), with curved-crystal graphite monochromator. The diffractometer was calibrated using a quartz standard, the National Institute of Standards and Technology (NIST) Standard Reference Material (SRM) 1878. Diffractograms were analyzed using the BrukerAXS EVA software (Bruker, Karlsruhe, Germany) package [44] and the International Center for Diffraction Data (ICDD) PDF-4 database.

Additional powdered samples were digested in concentrated aqua regia containing a 3:1 ratio of 37% HCl: 70% HNO_3 for 2 h at 95 °C and allowed to cool to 25 °C. Deionized water was added to each digest for a final 50 mL volume and was filtered using 0.45 µm pore-size filters. The digested samples were analyzed for soluble Ag, Au, Hg and Pb by Inductively Coupled Plasma-Atomic Emission Spectroscopy (ICP-AES) analysis using a Perkin-Elmer Optima 3300DV inductively coupled plasma-atomic emission spectrometer (Perkin-Elmer, Waltham, USA). Mercury and lead are often detected within acidic weathering environments and Au commonly occurs in association with Ag [1,45],

therefore, these elements were selected for analysis. All measurements were referenced to elemental standards purchased from Alfa Aesar (Ward Hill, USA). Detection limits for were: 1.0 $\mu g \cdot g^{-1}$ Ag, 30 $\mu g \cdot g^{-1}$ Hg and 35 $\mu g \cdot g^{-1}$ Pb, 12.5 $\mu g \cdot g^{-1}$ Au. Gossans with the highest Ag content were triaged for micro-analysis since these samples represent the "oldest" type of regolith material that would contain chemical and structural evidence of Ag cycling. Terrace iron formations with the highest Ag content were used for microbial enrichments because these "younger" regolith materials occurred within mines sites where running water would support microbial life.

Gossan from the San Telmo mine was made into a polished thin-section for Electron Microprobe (EMP) and Scanning Electron Microscopy-Energy Dispersive Spectroscopy (SEM-EDS) analysis. The distribution of selected elements was obtained using a Cameca SXFive Electron Microprobe (Cameca, Gennevilliers, France) operating at 20 kV and 100 nA with five wavelength dispersive spectrometers calibrated to FeKα (LLIF), PbMα (LPET), AgLα (LPET), AuMα (PET) and HgLα (LLIF). Elemental maps were produced using a 1 μm step size with 50 ms dwell time. Regions containing higher detections of Ag were further analyzed using a JEOL JSM-7100F Field Emission Gun-Scanning Electron Microscope (SEM) (JEOL, Tokyo, Japan) to characterize micrometer-scale structures. The SEM, operating at 15 kV, was equipped with an energy dispersive detector.

2.3. Microbial Enrichments and Enumeration

Terrace iron formations from the Tharsis mine was the source for an iron-oxidizing microbial consortium. Primary enrichments were made in sterile 13 mm × 100 mm borosilicate glass test tubes by inoculating ca. 0.5 g of terrace iron formations into 4.5 mL of filter-sterilized (0.45 μm pore-size), basal salts growth medium [11]. Growth medium contained 3.03 mM $(NH_4)_2SO_4$, 0.57 mM K_2HPO_4, 1.62 mM $MgSO_4 \cdot 7H_2O$, 0.12 M $FeSO_4 \cdot 7H_2O$ with pH adjusted to 3.9 using H_2SO_4 to correspond with the average pH measured in the field. The enrichments were covered with push caps to maintain aerobic conditions and were placed in a non-shaking incubator at 23 °C for 3 weeks to ensure abundant microbial growth. Two sequential transfers were made by inoculating 0.5 mL of the preceding enrichment into 4.5 mL "fresh" growth medium. These transfers were incubated under the same condition to obtain microbial enrichments that no longer contained the original terrace iron formation inoculum. After three weeks of incubation, the pH of these microbial enrichments were measured using a Denver Instrument Basic pH Meter calibrated to pH 2, 4 and 7 reference standards. Uncertainty in pH measurements were ±0.1 pH units. Using the same growth medium previously described, a five-tube Most Probable Number (MPN) statistical method [46] was performed to estimate the number of iron-oxidizing microbes from the original terrace iron formations as well as the microbial enrichments. Positive growth was indicated by the formation of an iron oxyhydroxide mineral precipitate [11,27]. An abiotic control was also performed in parallel.

2.4. Microbial Enrichment-Ag System Experiments

A measured 24 mM Ag stock solution was prepared by dissolving 99.9% pure $AgNO_3$ into distilled, deionized water and was made into a 2 serial, ten-fold dilution. These Ag stock solutions were filtered and added to three-week-old microbial enrichments to examine the effect of iron-oxidizing bacteria/archaea on the stability of soluble Ag. At the start of this experiment, microbial enrichment-Ag systems contained final concentrations of 2.4, 0.24 and 0.024 mM Ag. These microbial enrichment-Ag systems were mixed by vortex, wrapped in aluminum foil to prevent any photocatalytic effects, performed in quadruplicate, and allowed to react for one week at 23 °C.

Additional microbial enrichments were passed through a 0.45 μm pore-size filter to separate cells and mineral precipitates from the fluid phase. The filtrates were used for mineralogical and electron microscopy analysis (see below) and the filtered solutions, i.e., "spent" medium, were used to make chemical controls. Spent medium-Ag systems were made by adding Ag stocks to the filtered solutions to have final concentrations of 2.4, 0.24 and 0.024 mM Ag. These spent medium-Ag systems were wrapped in aluminum foil, incubated under the same conditions as the microbial

enrichment-Ag systems and performed in triplicate. After one week of incubation, the pH of the microbial enrichment- and spent medium-Ag systems was measured. Both types of experimental Ag systems were filtered to separate solid constituents from the fluid phases. The filtered solutions, as well as the Ag stock solutions, were acidified with nitric acid and analyzed by ICP-AES for residual soluble Ag. The detection limit of Ag was 0.04 μM.

Filtrates from microbial enrichments and microbial enrichment-Ag systems were rinsed with distilled, deionized water and air-dried at 23 °C for 24 h. Micro X-ray Diffraction (μXRD) data of these filtrates were collected in coupled scan geometry using a Bruker D8 Discover microdiffractometer (Bruker, Billerica, MA, USA) operating at 40 kV and 40 mA with a Cu sealed tube source (Cu Kα, λ = 1.5418 Å), Göbel mirror parallel-beam optics, and 500 μm collimator snout, and 20 minutes integration time per frame. Diffracted X-rays were detected with a two-dimensional General Area Diffraction Detection System (GADDS). The μXRD data were analyzed using the BrukerAXS EVA software package [44] and the International Centre for Diffraction Data (ICDD) PDF-4 database.

Additional filtrates from microbial enrichments, microbial enrichment-Ag systems and spent medium-Ag systems were prepared as whole-mounts and ultrathin sections [31] for SEM-EDS and Transmission Electron Microscopy-Energy Dispersive Spectroscopy (TEM-EDS) analysis, respectively. See Shuster et al. (2014) for details on sample method preparation. Whole-mount samples were characterized using a LEO Zeiss 1540XB FEG-SEM (Zeiss, Oberkochen, Germany) with Oxford Instrument INCAx-sight EDS detector operating at 1 or 15 kV. Ultrathin sections were analyzed using a Phillips CM-10 transmission electron microscope (Phillips, Amsterdam, The Netherlands) operating at 80 kV.

The last replicate of the microbial enrichment-Ag systems were transferred to fresh growth medium to determine if iron-oxidizing bacteria/archaea could be re-cultured after the exposure to soluble Ag. These recovery enrichments were prepared in the same method and incubated under the same conditions as the original microbial enrichments. A five-tube MPN was also performed to estimate how many cells were likely to be metabolically active in the recovery enrichment.

3. Results

3.1. Chemistry, Mineralogy and Structure of Regolith Materials

Based on XRD analysis, gossans were primarily composed of goethite and hematite with a lesser detection of metal sulfides and quartz. Silver, in the form of argentojarosite, was detected in gossan from San Telmo. Terrace iron formations were primarily comprised of hydroniumjarosite and schwertmannite with a lesser detection of gypsum. Of the three different types of regolith materials, mine soils contained a broader range of minerals including: iron oxyhydroxides, clays and soluble sulfate salts. See Table 1 for detailed mineralogical composition.

The highest Ag concentration of 4.01×10^2 μg·g^{-1} Ag, based on ICP-AES analysis, was detected in gossan from the San Telmo mines at ca. 7 and 47 times greater relative to gossans from the Tharsis and San Miguel mines, respectively. Terrace iron formations from Tharsis contained the highest Ag concentration (27.6 μg·g^{-1} Ag) and was ca. 6 and 11 times greater than the detections from San Miguel and San Telmo, respectively. Mine soils contained the least amount and the smallest range of Ag concentrations. Like the Ag concentrations, the greatest detection and broadest range of Hg and Pb occurred within gossans whereas and lesser detections and smaller ranges of Hg and Pb occurred within terrace iron formations and mine soils (Table 2). There was no detection of Au from any of the regolith materials.

Table 1. Identification and semi-quantitative abundances of minerals comprising gossan, terrace iron formations and mine soils based on XRD analysis.

Type of Regolith Material *Sample Location*	Major Minerals (ca. 25–100 vol %)	Minor Minerals (ca. 5–20 vol %)
Gossans		
San Telmo	goethite hematite quartz galena	argentojarosite plumbojarosite jarosite
San Miguel	goethite hematite pyrite	barite quartz
Tharsis	goethite quartz pyrite	hematite jarosite
Terrace iron formations		
San Telmo	schwertmannite hydroniumjarosite	quartz gypsum
San Miguel	schwertmannite	hydroniumjarosite gypsum
Tharsis	schwertmannite hydroniumjarosite	gypsum pyrite quartz
Mine soils		
San Telmo	bernalite copiapite goethite	melanterite
San Miguel	copiapite goethite hydroniumjarosite quartz	kaolinite
Tharsis	goethite hydroniumjarosite kaolinite	coquimbite

Table 2. The Ag, Hg and Pb concentrations within gossan, terrace iron formations and mine soils based on ICP-AES analysis.

Type of Regolith Material *Sample Location*	Ag ($\mu g \cdot g^{-1}$)	Hg ($\mu g \cdot g^{-1}$)	Pb ($\mu g \cdot g^{-1}$)
Gossans			
San Telmo	4.01×10^2	7.04×10^2	1.22×10^4
San Miguel	8.50	2.14×10^2	2.0×10^3
Tharsis	56.7	53.4	2.52×10^3
Terrace iron formations			
San Telmo	2.46	<30	1.29×10^3
San Miguel	4.60	31.7	2.59×10^2
Tharsis	27.6	58.4	8.14×10^3
Mine soils			
San Telmo	3.64	<30	2.28×10^2
San Miguel	1.86	<30	1.23×10^2
Tharsis	1.69	<30	95.1

Gossan from San Telmo contained regions that were either consolidated or unconsolidated. Consolidated regions were characterized by having iron-oxide minerals, which occurred as a dense matrix, whereas unconsolidated regions contained iron-oxide minerals that appeared to have a greater amount of interstitial space between mineral grains. Silver, detectable by backscatter (BSC) SEM analysis, occurred as a Ag-Cl mineral at the boundary between these two regions. The distribution of Ag was also closely associated with Hg and Pb sulfide minerals (Figure 2A,B). Although Au was not detected by ICP-AES or EMP analysis, Au nanoparticles were observed in association with Ag-Cl minerals within the iron-oxide mineral matrix (Figure 2C). Unconsolidated regions contained micrometer-scale euhedral crystals of plumbojarosite. Some crystals appeared to be "coated" with nanometer-scale acicular iron-oxide minerals (Figure 2D). Crevices within consolidated regions contained clusters of circular and oval structures that were 1 to 2 μm in size. These structures appeared as nanometer-thick "rings" or as oval-shaped molds within the iron-oxide mineral matrix (Figure 3).

3.2. Biogeochemical Reduction of Ag

Based on the MPN statistical method, the terrace iron formations and microbial enrichments contained 3.5×10^3 cells·g^{-1} and 5.4×10^7 cells·mL^{-1}, respectively. The abiotic controls should no growth. The microbial enrichments formed hydroniumjarosite and schwertmannite and the pH decreased from 3.9 to 2.4. These phenotypic changes along with increased microbial number indicated growth of actively metabolizing iron-oxidizing bacteria/archaea [11,21]. Hydroniumjarosite occurred as micrometer-scale euhedral crystals whereas schwertmannite occurred as poorly-crystalline, pseudo-acicular minerals (Figure 4A). Some cells appeared to be extensively mineralized in schwertmannite (Figure 4B). This mineral appeared to nucleate on the extracellular surface of the cell and grow radially. A lesser amount of pseudo-acicular schwertmannite occurred within the intracellular space. Mineralization of microbial cells preserved the cell wall structure thereby retaining the circular to oval-shape morphology (Figure 4C).

After the addition of Ag to the microbial enrichments and the spent medium, the fluid phases of both systems changed from a transparent, red-orange color to clear within an hour. After one week of incubation, the microbial enrichment-Ag systems removed $35 \pm 2\%$ more Ag from solution in comparison to the spent medium-Ag systems (Figure 5A). Silver concentrations within the stock solution remained unchanged after one week. The detection of hydroniumjarosite by μXRD analysis shifted to argentojarosite with increasing Ag concentrations in the microbial enrichment-Ag systems. Argentojarosite occurred as euhedral, nanometer- to micrometer-scale minerals (Figure 5B). Similarly, the formation of argentojarosite within the spent medium-Ag systems was confirmed by SEM-EDS analysis (Figure 5C). After three weeks of incubation, the recovery enrichment and MPN indicated that only 0.23×10^2 cells·mL^{-1} were recovered from the microbial enrichment-Ag system exposed to 0.024 mM Ag. Metabolically active microbes from the recovery enrichments was inferred by the formation of hydroniumjarosite/schwertmannite precipitation.
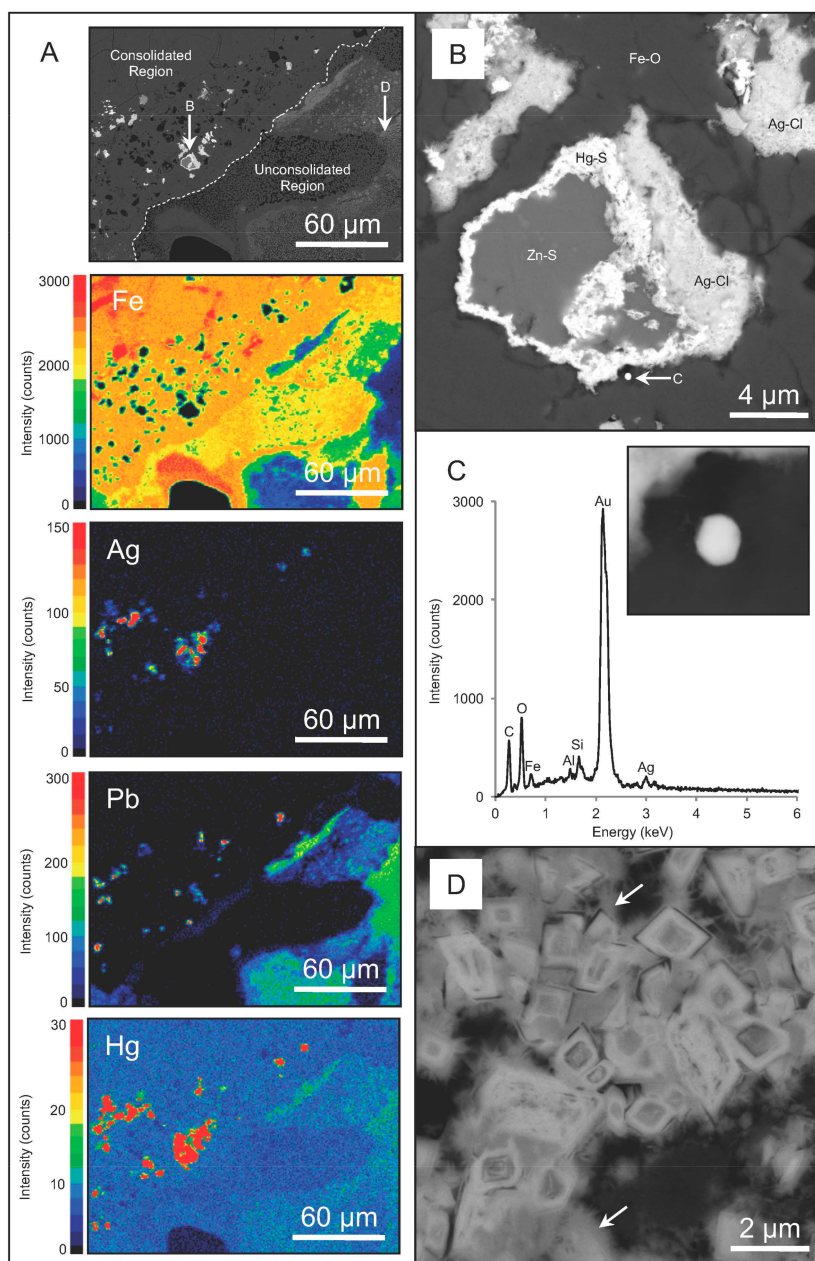
Figure 2. A low-resolution BSC SEM micrograph demonstrating the consolidated and unconsolidated region within gossan and corresponding EMP maps highlighting the distribution of Ag, Fe, Pb and Hg. Silver occurred in close association with mercury (**A**); a high-resolution BSC SEM micrographs of a secondary Ag-bearing minerals and a secondary, gold nanoparticle within the consolidated regions (**B**,**C**). A high-resolution BSC SEM micrograph of euhedral plumbojarosite coated with acicular; iron-oxidehydroxide minerals (arrows, **D**).
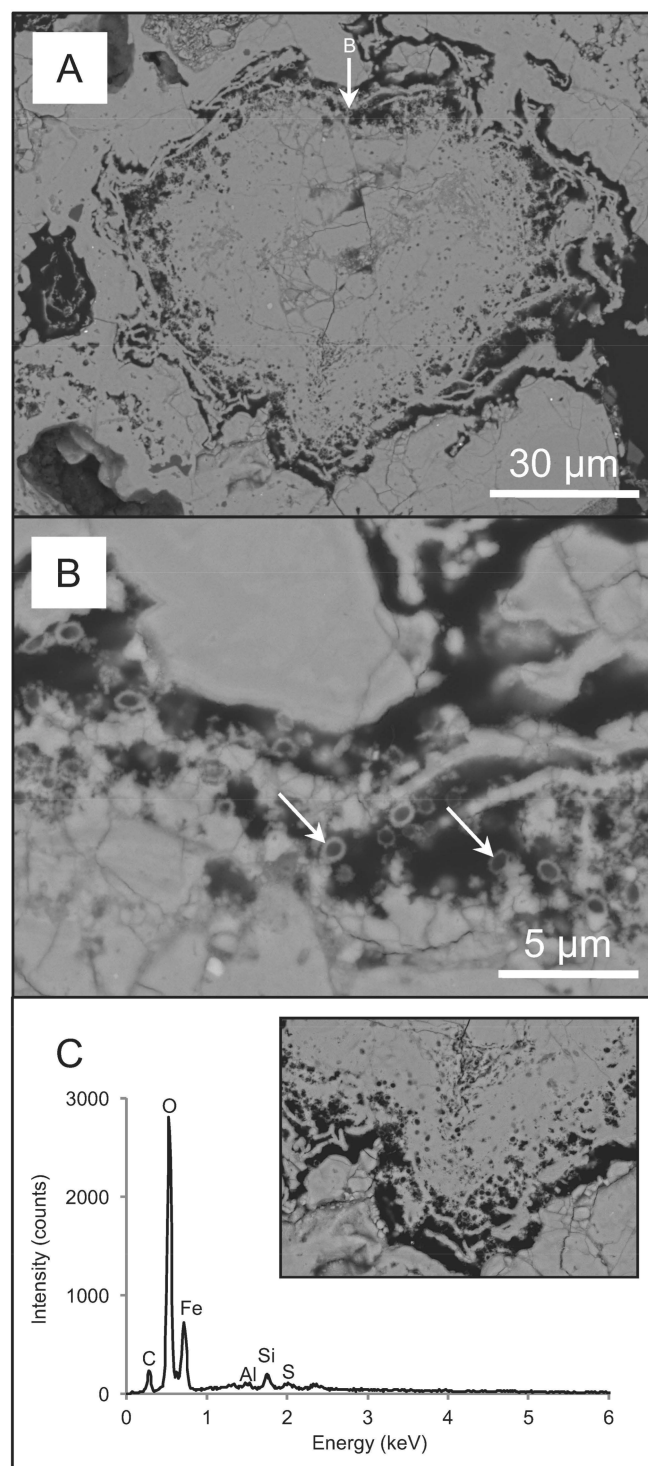
Figure 3. A low-resolution BSC SEM micrograph of a crevice containing an abundance of hollow, circular and oval-shaped structures (**A**); a high-resolution BSC SEM micrograph of these structures that were interpreted as microbial microfossils that once comprised a biofilm within the crevices of gossan (**B**); a representative EDS spectrum identifying the elemental composition of the region containing microfossils (**C**, inset).
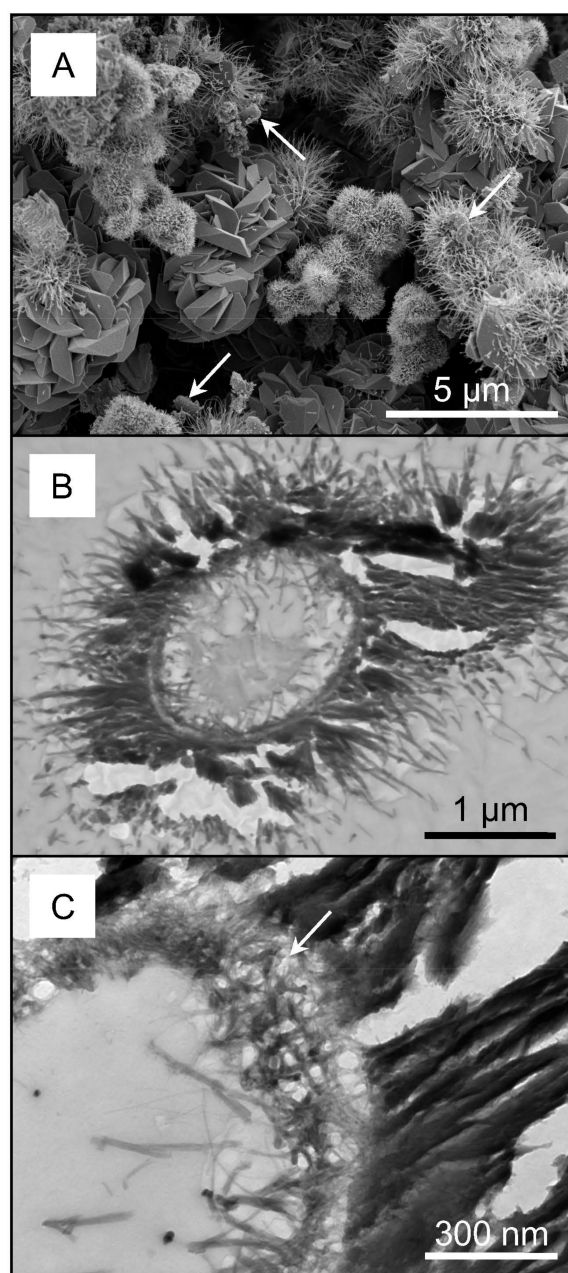
Figure 4. A low-resolution SE SEM micrograph of euhedral hydronium jarosite and poorly-crystalline, i.e., pseudo-acicular, schwertmannite and cells (arrows) from the microbial enrichments (**A**); a low-resolution TEM micrograph of a bacterium extensively mineralized pseudo-acicular schwertmannite (**B**); a high-resolution TEM micrograph demonstrating the preservation of the cell wall (arrow, **C**) and the lesser amount of intracellular mineralization relative to the extracellular surface (**C**).
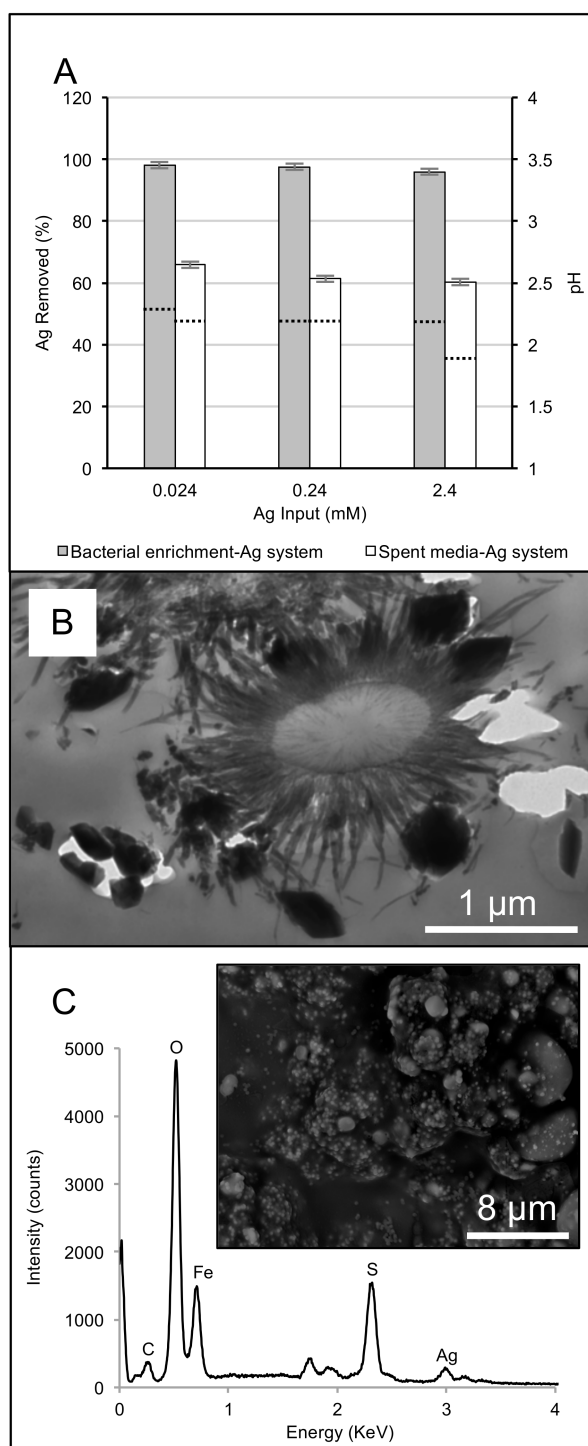
Figure 5. Average percent of Ag removed by the microbial enrichment- and spent medium-Ag systems based on ICP-AES analysis. Dashed lines represent pH within the corresponding experimental system (**A**); a high-resolution TEM micrograph of a mineralized cell and nanometer-scale argentojarosite from a microbial enrichment-Ag system exposed to 2.40 mM Ag (**B**); a low resolution BSC SEM micrograph and representative EDS spectrum of a spent medium-Ag system exposed to 2.40 mM Ag that precipitated argentojarosite. The unlabeled peaks are residual Si from the test tube and Os deposition for reducing charging, respectively (**C**).
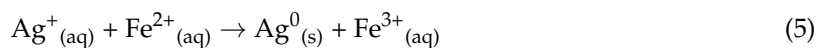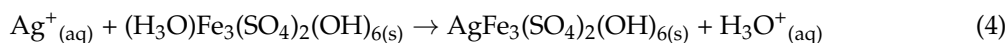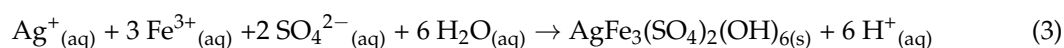
4. Discussion

4.1. Interpretations of Ag Biogeochemical Cycling within Regolith Materials

From a biogeochemical perspective, gossans represent older regolith material while terrace iron formations and mine soils represented younger regolith materials in which Ag could be mobilized. Iron-oxyhydroxide and sulfate-bearing minerals comprised the majority of gossans, terrace iron formations and mine soils. While this mineralogical composition reflects the redox conditions contributing to the formation of these regolith materials [24,45,47–50], variations in Ag concentrations highlight the dissolution, mobility and re-precipitation of Ag within this environment. Relative to terrace iron formations and mine soils, gossans contained both a chemical and a structural 'record' of past biogeochemical processes promoting precious metal mobility. While plumbojarosite and argentojarosite ($(Pb/Ag)Fe_{3-6}(SO_4)_{2-4}(OH)_{6-12}$) were detected in the San Telmo gossan, the observation of Ag halide minerals, e.g., chlorargyrite ($AgCl$) suggests that the chemical composition of percolating groundwater through gossan were variable. Residual zinc sulfide minerals could have acted as a selective precipitant for dissolved Hg forming an insoluble mercury sulfide [51] and thereby immobilizing dissolved Ag as a separate precipitate (Figure 2). The presence of gold nanoparticles also exemplifies the biomobility of precious metals within gossan since soluble gold complexes are generally unstable under inorganic/chemical weathering conditions [31,32,52]. Crevices within gossan allows groundwater to descend and provides ideal microenvironments for microbial attachment and growth [53–55]. With regard to iron biogeochemical cycling, microorganisms are known to contribute to the structure of terrace iron formations as well as other ferruginous duricrust such as canga [43,56,57]. Circular and oval structures within gossan (Figure 3) were interpreted as microbial microfossils based on the mode of biomineralization and cell wall preservation observed from the microbial enrichments (Figure 4A–C). Therefore, microbial communities contributed to the structure of gossan and presumably the geochemical conditions promoting Ag cycling. It is reasonable to suggest that these processes would also occur within terrace iron formations and mine soils so long as water is available to support microbial life.

4.2. Microbially-Catalyzed Ag Immobilization

Terrace iron formation was a source of metabolically active iron-oxidizing microbes for the experimental systems that favored the formation of argentojarosite. The complexation of soluble Ag^+ with excess Fe^{3+} and SO_4^{2-} resulting in the formation of argentojarosite was likely the reaction mechanism in both the microbial enrichment- and spent medium-Ag systems (Reaction (3)) [25]. The decrease in pH that occurred after the addition of soluble Ag^+ to both experimental systems, could be attributed to this acid-producing reaction. Since the microbial enrichment-Ag system contained hydroniumjarosite, Ag^+ substitution of H_3O^+ in the A-site of hydroniumjarosite (Reaction (4)) [25] likely also occurred and would explain the removal of ca. 35% more Ag relative to the spent medium-Ag system. In both experimental systems, the color change of the fluid phase after 1 h suggests that the rate of argentojarosite precipitation likely occurred more rapidly relative to the rate of Ag^+ substitution into hydroniumjarosite in the microbial enrichment-Ag system. In addition, it is possible that Ag^+ could have also been reduced by residual Fe^{2+} in both experimental systems (Reaction (5)). Increased metal concentrations are known to cause cell lyses thereby releasing intracellular material that could act as additional reductants that contribute to the formation of Ag (and Au) nanoparticles (Reaction (6)) [58–60]. In the natural environment, however, Ag nanoparticles would likely be unstable for prolonged periods of time as they would also be subjected to dissolution processes [61–64]. Cell lysing can also act as a buffering mechanism and could explain the difference in pH between the microbial enrichment- and spent medium-Ag systems [65,66]. The recovery enrichments demonstrated

that Ag concentrations greater than 0.024 mM Ag were lethal, which is consistent with tolerable Ag concentrations for *A. ferrooxidans* [66].

$$Ag^+_{(aq)} + 3\ Fe^{3+}_{(aq)} + 2\ SO_4{}^{2-}_{(aq)} + 6\ H_2O_{(aq)} \rightarrow AgFe_3(SO_4)_2(OH)_{6(s)} + 6\ H^+_{(aq)} \tag{3}$$

$$Ag^+_{(aq)} + (H_3O)Fe_3(SO_4)_2(OH)_{6(s)} \rightarrow AgFe_3(SO_4)_2(OH)_{6(s)} + H_3O^+_{(aq)} \tag{4}$$

$$Ag^+_{(aq)} + Fe^{2+}_{(aq)} \rightarrow Ag^0_{(s)} + Fe^{3+}_{(aq)} \tag{5}$$

$$Ag^+_{(aq)} + CHO_2{}^-_{(s)} \rightarrow Ag^0_{(s)} + CHO_{2(s)} \tag{6}$$

4.3. Temporal Estimates of Ag Biogeochemical Cycling

Biogeochemical cycling of Ag under acidic weathering conditions involves the dissolution of Ag from primary, Ag-bearing minerals such as (Hg/Au)-Ag-alloys or Ag-bearing sulfides. This dissolution is counterbalanced by re-precipitation of secondary, Ag-bearing minerals or elemental Ag [2]. Under weathering conditions, thiosulfate is considered an important ligand for the mobility of soluble Ag within hydrological regimes, where metal sulfides are abundant (Reactions (7) and (8)) [1,16,67–70]. Silver dissolution can be considered a rate-limiting process for Ag cycling because argentojarosite formation occurs rapidly under similar biogeochemical conditions. For estimating the kinetics of Ag biogeochemical cycling, the mass of Ag within each type of regolith material was interpreted as the amount of Ag that had undergone dissolution and re-precipitation. For this model, thiosulfate-leaching was used as a simplified biogeochemical mechanism for Ag dissolution [71]. Within acidic weathering environments, the majority of dissolved sulfur occurs as sulfate, i.e., average 0.08 mM[45], whereas thiosulfate is a transitory ligand that occurs at trace concentrations, i.e., ca. 0.05% of total dissolved solved sulfur [22]. The dissolution rate of Ag has been estimated to be approximately 37.5 µg min^{-1} using 0.4 M thiosulfate under alkaline conditions (pH 10) [72]. This thiosulfate concentration and pH, however, are approximately 1.03×10^6 times and 7.7 times greater, respectively, than what would naturally occur in the weathering environment of the abandoned mine sites. Together, these values represent Ag dissolution rate factors because Ag dissolution is dependent on thiosulfate concentrations and its stability. Furthermore, the formation of thiosulfate through microbially-catalyzed metal sulfide oxidation is variable because the metabolic efficiency of iron-oxidizing microbes is also variable, i.e., 3.2% [73], 20.5% [11] or 30% [74] metabolic efficiency. For the kinetic calculation, an average 10.5% metabolic efficiency was used. Therefore, gossans represented 0.6–146.7 years of Ag biogeochemical cycling, whereas terrace iron formations ranged between 1.9 and 42.7 years and mine soils ranged between 0.7 and 1.6 years (Table 3). While these ranges of time could reflect the duration of which these regolith materials were emplaced, they suggest a continuum of biogeochemical Ag cycling between different types of regolith materials. Water percolating through gossan crevices, over terrace iron formations and within pore spaces of mine soils would sustain microbial metabolism thereby contributing to Ag dissolution and re-precipitation. Furthermore, it is reasonable to suggest that the lower-range values could reflect seasonal variations in precipitation [75] whereas higher-range values could represent the extent to which Ag biogeochemical cycling occurs within the respective regolith material. In terms of environmental reclamation, historical mining practices have left behind a legacy that pose a risk of silver contamination and toxicological effects on the surrounding environment [76,77]. This contamination can be attributed, in part, to inefficient methods of extraction based on today's standards [78]. Understanding precious metal mobility could help reconcile the increasing demand for precious metals by using mine "wastes" as a resource whilst remediating mine sites to reduce the negative impact on the environment.
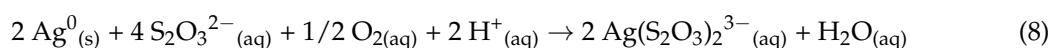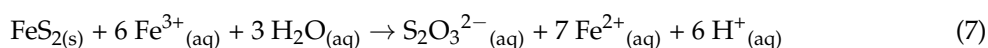
$$FeS_{2(s)} + 6\ Fe^{3+}_{(aq)} + 3\ H_2O_{(aq)} \rightarrow S_2O_3{}^{2-}_{(aq)} + 7\ Fe^{2+}_{(aq)} + 6\ H^+_{(aq)} \tag{7}$$

$$2\ Ag^0_{(s)} + 4\ S_2O_3{}^{2-}_{(aq)} + 1/2\ O_{2(aq)} + 2\ H^+_{(aq)} \rightarrow 2\ Ag(S_2O_3)_2{}^{3-}_{(aq)} + H_2O_{(aq)} \tag{8}$$

Table 3. Calculations for estimating the length of time for Ag dissolution and re-precipitation, i.e., cycling, to occur within gossans, terrace iron formations and mine soils based on Ag concentrations determined by ICP-OES.

Type of Regolith Material *Sample Location*	Sample Mass (g)	Ag Mass (μg) [A]	Time (Years) [B]
Gossans			
San Telmo	5.06	2.03×10^3	1.46×10^3
San Miguel	1.03	8.78	0.63
Tharsis	11.4	6.44×10^2	46.4
Terrace iron formations			
San Telmo	10.8	26.5	1.91
San Miguel	29.9	1.37×10^2	9.9
Tharsis	21.5	5.93×10^2	42.7
Mine soils			
San Telmo	6.25	6.25	1.64
San Miguel	6.62	6.62	0.89
Tharsis	5.58	5.58	0.68

[A] Mass of Ag = sample mass $\times$ Ag concentration measured by ICP-OES (Table 2); [B] years for Ag dissolution/re-precipitation = (A $\div$ 37.5 μM·Ag·min^{-1}) $\times$ (7.93×10^6) $\times$ (17.9%) $\div$ 525,600 min·year^{-1}. Where 7.93×10^6 is the dissolution rate factor and 17.9% is the metabolic efficiency of iron-/sulfur-oxidizing bacteria.

5. Conclusions

While gossans contain the greatest amount of Ag, the occurrence of Ag within terrace iron formations and mine soils highlights the extent of Ag mobility within younger regolith materials. Structural characterization of gossan revealed that different mechanisms of Ag cycling likely occurred contemporaneously within gossan. More importantly, microfossils preserved within crevices suggest that resident microorganisms likely contributed to the biogeochemical conditions promoting Ag cycling. The precipitation of argentojarosite from solution or the substitution of Ag cations into microbially-formed hydroniumjarosite occurred fairly quickly in the microbial enrichment-Ag systems. These mechanisms of Ag immobilization suggest that the stability of soluble Ag in acidic, weathering environments would be brief and that Ag dissolution would likely be the rate-limiting factor in Ag biogeochemical cycling. Furthermore, calculations estimating the kinetics of biogeochemical Ag cycling suggest that Ag dissolution and re-precipitation is a continuous. This study provides insight on the dynamics of Ag biogeochemical cycling in relation to its mobility and dispersion within different types of regolith materials typical found in acidic, weathering environments of abandoned mines.

Author Contributions: J.S. and M.R.M.I. were PhD students at Western University under the supervision of supervision of G.S. (Shuster) and R.L.F. and N.R.B. (Izawa), respectively. This collaborative research project was developed as part of the 2008-2009 International Field School (IFS) led by N.R.B. Participation of J.S. and M.R.M.I. in IFS enabled sampling of natural regolith materials. J.S. and M.R.M.I conducted microbial enrichments and microanalyses. J.S. is now a postdoctoral research fellow under the mentorship of F.R. Funding granted to R.L.F., N.R.B., G.S. and F.R. made this research collaboration possible.

References

1. Boyle, R.W. The geochemistry of silver and its deposits. *Geol. Surv. Can. Bull.* **1968**, *160*, 1–282.
2. Sillitoe, R.H. Supergene silver enrichment reassessed. *Soc. Econ. Geol. Spec. Pub.* **2009**, *14*, 15–32.
3. Steger, H.F.; Desjardins, L.E. Oxidation of sulfide minerals, 4. Pyrite, chalcopyrite and pyrrhotite. *Chem. Geol.* **1978**, *23*, 225–237. [CrossRef]
4. Lowson, R.T. Aqueous oxidation of pyrite by molecular oxygen. *Chem. Rev.* **1982**, *82*, 461–496. [CrossRef]
5. Buckley, A.N.; Walker, G.W. The surface composition of arsenopyrite exposed to oxidising environments. *Appl. Surf. Sci.* **1988**, *35*, 227–240. [CrossRef]
6. Nesbitt, H.W.; Muir, I.J.; Pratt, A.R. Oxidation of arsenopyrite by air and air-saturated, distilled water, and implications for mechanism of oxidation. *Geochim. Cosmochim. Acta* **1995**, *59*, 1773–1786. [CrossRef]
7. Chandra, A.P.; Gerson, A.R. The mechanisms of pyrite oxidation and leaching: A fundamental perspective. *Surf. Sci. Rep.* **2010**, *65*, 293–315. [CrossRef]
8. Nordstrom, D.K. Aqueous pyrite oxidation and the consequent formation of secondary iron minerals. In *Acid Sulfate Weathering*; Kittrick, J.A., Fanning, D.S., Hosner, L.R., Eds.; Soil Science Society of America: Madison, WI, USA, 1982; pp. 37–56.
9. Nordstrom, D.K.; Alpers, C. Negative pH, efflorescent mineralogy, and consequences for environmental restoration at the Iron Mountain Superfund site, California. *Proc. Natl. Acad. Sci. USA* **1999**, *96*, 3455–3462. [CrossRef] [PubMed]
10. Singer, P.C.; Stumm, W. Acidic mine drainage: The rate-determining step. *Science* **1970**, *167*, 1121–1123. [CrossRef] [PubMed]
11. Silverman, M.P.; Lundgren, D.G. Studies on the chemoautotrophic iron bacterium *Ferrobacillus ferrooxidans*. *J. Bacteriol.* **1959**, *77*, 642–647. [PubMed]
12. Shuster, J.; Lengke, M.F.; Márquez-Zavalía, M.F.; Southam, G. Floating gold grains and nanophase particles produced from the biogeochemical weathering of a gold-bearing ore. *Econ. Geol.* **2016**, *111*, 1485–1494. [CrossRef]
13. Mann, A.W. Mobility of gold and silver in lateritic weathering profiles: Some observations from Western Australia. *Econ. Geol.* **1984**, *79*, 38–49. [CrossRef]
14. Webster, J.G.; Mann, A.W. The Influence of climate, geomorphology and primary geology on the supergene migration of gold and silver. *J. Geochem. Explor.* **1984**, *22*, 21–42. [CrossRef]
15. Craw, D.; MacKenzie, D.J. Near-surface secondary gold mobility and grain-size enhancement, Barewood Mine, east Otago, New Zealand. *N. Z. J. Geol. Geophys.* **2010**, *35*, 151–156. [CrossRef]
16. Craw, D.; Lilly, K. Gold nugget morphology and geochemical environments of nugget formation, southern New Zealand. *Ore Geol. Rev.* **2016**, *79*, 301–315. [CrossRef]
17. Reith, F.; Lengke, M.F.; Falconer, D.; Craw, D.; Southam, G. The geomicrobiology of gold. *ISME J.* **2007**, *1*, 567–584. [CrossRef] [PubMed]
18. Brugger, J.; Etschmann, B.; Grosse, C.; Plumridge, C.; Kaminski, J.; Paterson, D.; Shar, S.S.; Ta, C.; Howard, D.L.; de Jonge, M.D.; et al. Can biological toxicity drive the contrasting behavior of platinum and gold in surface environments? *Chem. Geol.* **2013**, *343*, 99–110. [CrossRef]
19. Greffie, C.; Benedetti, M.F.; Parron, C.; Amouric, M. Gold and iron oxide associations under supergene conditions: An experimental approach. *Geochim. Cosmochim. Acta* **1996**, *60*, 1531–1542. [CrossRef]
20. Webster, J.G. The solubility of gold and silver in the system Au-Ag-S-O_2-H_2O at 25 °C and 1 atm. *Geochim. Cosmochim. Acta* **1986**, *50*, 1837–1845. [CrossRef]
21. Nordstrom, D.K.; Southam, G. Geomicrobiology of sulphide mineral oxidation. *Rev. Mineral.* **1997**, *35*, 362–390.
22. Schippers, A.; Sand, W. Bacterial leaching of metal sulfides proceeds by two indirect mechanisms via thiosulfate or via polysulfides and sulfur. *Appl. Environ. Microbiol.* **1999**, *65*, 319–321. [PubMed]
23. Groat, L.A.; Jambor, J.L.; Pemberton, B.C. The crystal structure of argentojarosite, $AgFe_3(SO_4)_2(OH)_6$. *Can. Mineral.* **2003**, *41*, 921–928. [CrossRef]
24. Amorós, J.; Lunar, R.; Tavira, P. Jarosite: A silver bearing mineral of the gossan of Rio Tinto (Huelva) and la Union (Cartagena, Spain). *Miner. Depos.* **1981**, *16*, 205–213. [CrossRef]
25. Sasaki, K.; Tsunekawa, M.; Konno, H. Characterisation of argentojarosite formed from biologically oxidised Fe^{3+} ions. *Can. Mineral.* **1995**, *33*, 1311–1319.

26. Sasaki, K.; Sakimoto, T.; Endo, M.; Konno, H. FE-SEM study of microbially formed jarosite by *Acidithiobacillus ferrooxidans*. *Mater. Trans.* **2006**, *47*, 1155–1162. [CrossRef]

27. Sasaki, K.; Konno, H. Morphology of jarosite-group compounds precipitated from biologically and chemically oxidized Fe ions. *Can. Mineral.* **2000**, *38*, 45–56. [CrossRef]

28. Wang, H.; Bigham, J.M.; Tuovinen, O.H. Formation of schwertmannite and its transformation to jarosite in the presence of acidophilic iron-oxidizing microorganisms. *Mater. Sci. Eng. C Mater.* **2006**, *26*, 588–592. [CrossRef]

29. Liao, Y.; Zhou, L.; Liang, J.; Xiong, H. Biosynthesis of schwertmannite by *Acidithiobacillus ferrooxidans* cell suspensions under different pH condition. *Mater. Sci. Eng. C Mater.* **2009**, *29*, 211–215. [CrossRef]

30. Daoud, J.; Karamanev, D. Formation of jarosite during Fe^{2+} oxidation by *Acidithiobacillus ferrooxidans*. *Miner. Eng.* **2006**, *19*, 960–967. [CrossRef]

31. Shuster, J.; Bolin, T.; MacLean, L.C.W.; Southam, G. The effect of iron-oxidising bacteria on the stability of gold (I) thiosulfate complex. *Chem. Geol.* **2014**, *376*, 52–60. [CrossRef]

32. Shuster, J.; Marsden, S.; Maclean, L.; Ball, J.; Bolin, T.; Southam, G. The immobilization of gold from gold (III) chloride by a halophilic sulfate-reducing bacterial consortium. *Geol. Soc. Lond. Spec. Publ.* **2013**, *393*, 249–263. [CrossRef]

33. Relvas, J.M.; Tassinari, C.C.; Munhá, J.; Barriga, F.J. Multiple sources for ore-forming fluids in the Neves Corvo VHMS Deposit of the Iberian Pyrite Belt (Portugal): Strontium, neodymium and lead isotope evidence. *Miner. Depos.* **2001**, *36*, 416–427. [CrossRef]

34. Strauss, G.; Rober, G.; Lecolle, M.; Lopera, E. Geochemical and geological study of the volcano-sedimentary sulfide orebody of La Zarza, Huelva Province, Spain. *Econ. Geol.* **1981**, *76*, 1975–2000. [CrossRef]

35. Sáez, R.; Pascual, E.; Toscano, M.; Almodóvar, G. The Iberian type of volcano-sedimentary massive sulfide deposits. *Miner. Depos.* **1999**, *34*, 549–570.

36. Ruiz, C.; Arribas, A.; Arribas, A., Jr. Mineralogy and geochemistry of the Masa Valverde blind massive sulfide deposit, Iberian Pyrite Belt (Spain). *Ore Geol. Rev.* **2002**, *19*, 1–22. [CrossRef]

37. Tornos, F. Environment of formation and styles of volcanogenic massive sulfides: The Iberian Pyrite Belt. *Ore Geol. Rev.* **2006**, *28*, 259–307. [CrossRef]

38. Boyle, D.R. Oxidation of Massive Sulfide Deposits in the Bathurst Mining Camp, New Brunswick. In *Environmental Goechemistry of Sulfide Oxidation*; Alpers, C., Ed.; American Chemical Society Symposium Series: Washington, DC, USA, 1993; pp. 535–550.

39. Velasco, F.; Herrero, J.M.; Suárez, S.; Yusta, I.; Alvaro, A.; Tornos, F. Supergene features and evolution of gossans capping massive sulphide deposits in the Iberian Pyrite Belt. *Ore Geol. Rev.* **2013**, *53*, 181–203. [CrossRef]

40. Hutchinson, R.W. Precious metals in massive base metal sulphide deposits. *Geol. Rundsch.* **1990**, *79*, 241–262. [CrossRef]

41. Leistel, J.M.; Marcoux, E.; Deschamps, Y.; Joubert, M. Antithetic behaviour of gold in the volcanogenic massive sulphide deposits of the IPB. *Miner. Depos.* **1998**, *33*, 82–97. [CrossRef]

42. Tornos, F.; Solomon, M.; Conde, C.; Spiro, B.F. Formation of the Tharsis massive sulphide deposit, Iberian Pyrite Belt: Geological lithogeochemical, and stable isotope evidence for deposition in a brine pool. *Econ. Geol.* **2008**, *103*, 185–214. [CrossRef]

43. Sánchez España, J.; Santofimia Pastor, E.; López Pamo, E. Iron terraces in acid mine drainage systems: A discussion about the organic and inorganic factors involved in their formation through observations from the Tintillo acidic river (Riotinto mine, Huelva, Spain). *Geosphere* **2007**, *3*, 133–151. [CrossRef]

44. BrukerAXS. *DIFFRACplus Evaluation Package Release 2005*; Bruker AXS: Karlsruhe, Germany, 2005.

45. Sánchez España, J.; López Pamo, E.; Santofimia, E.; Aduvire, O.; Reyes, J.; Barettino, D. Acid mine drainage in the Iberian Pyrite Belt (Odiel river watershed, Huelva, SW Spain): Geochemistry, mineralogy and environmental implications. *Appl. Geochem.* **2005**, *20*, 1320–1356. [CrossRef]

46. Cochran, W.G. Estimation of bacterial densities by means of the "Most Probable Number". *Biometrics* **1950**, *6*, 105–116. [CrossRef] [PubMed]

47. España, J.S.; Pamo, E.L.; Pastor, E.S.; Andrés, J.R.; Rubí, J.A.M. The natural attenuation of two acidic effluents in Tharsis and La Zarza-Perrunal mines (Iberian Pyrite Belt, Huelva, Spain). *Environ. Geol.* **2005**, *49*, 253–266. [CrossRef]

48. Olías, M.; Nieto, J. Background Conditions and Mining Pollution throughout History in the Río Tinto (SW Spain). *Environments* **2015**, *2*, 295–316. [CrossRef]

49. Edwards, K.J.; Bond, P.L.; Druschel, G.K.; McGuire, M.M.; Hamers, R.J.; Banfield, J.F. Geochemical and biological aspects of sulfide mineral dissolution: Lessons from Iron Mountain, California. *Chem. Geol.* **2000**, *169*, 383–397. [CrossRef]

50. Velasco, F.; Tornos, F. Los sulfuros masivos (Cu-Zn-Au) de Lomero Poyatos (Faja Pirítica Iberica): Encuadre geológico, alteración hidrothermal y removilización. *Macla* **2006**, *6*, 489–492.

51. Gabby, K.L.; Eisele, T.C. Selective removal of mercury using zinc sulfide. *Miner. Metall. Process.* **2013**, *30*, 91–94.

52. Colin, F.; Vieillard, P.; Ambrosi, J.P. Quantitative approach to physical and chemical gold mobility in equitorial rainforest lateritic environment. *Earth Planet. Sci. Lett.* **1993**, *114*, 269–285. [CrossRef]

53. Golubic, S.; Friedmann, I.; Schneider, J. The lithobiontic ecological niche, with special reference to microorganisms. *J. Sediment. Petrol.* **1981**, *51*, 475–478.

54. Friedmann, I. Endolithic microorganisms in the Antarctic cold desert. *Science* **1982**, *215*, 1045–1053. [CrossRef] [PubMed]

55. Westall, F. The nature of fossil bacteria: A guide to the search for extraterrestrial life. *J. Geophys. Res. Planet.* **1999**, *104*, 16437–16451. [CrossRef]

56. Fernández-Remolar, D.C.; Knoll, A.H. Fossilization potential of iron-bearing minerals in acidic environments of Rio Tinto, Spain: Implications for Mars exploration. *Icarus* **2008**, *194*, 72–85. [CrossRef]

57. Levett, A.; Gagen, E.; Shuster, J.; Rintoul, L.; Tobin, M.; Vongsvivut, J.; Bambery, K.; Vasconcelos, P.; Southam, G. Evidence of biogeochemical processes in iron duricrust formation. *J. S. Am. Earth Sci.* **2016**, *71*, 131–142. [CrossRef]

58. Tsezos, M.; Remoudaki, E.; Angelatou, V. Biosorption sites of selected metals using eletron microscopy. *Comp. Biochem. Physiol.* **1997**, *118*, 481–487. [CrossRef]

59. Lin, Z.; Zhou, C.; Wu, J.; Zhou, J.; Wang, L. A further insight into the mechanism of Ag^+ biosorption by *Lactobacillus* sp. strain A09. *Spectrochim. Acta A* **2005**, *61*, 1195–1200. [CrossRef] [PubMed]

60. Li, L.; Hu, Q.; Zeng, J.; Qi, H.; Zhuang, G. Resistance and biosorption mechanism of silver ions by *Bacillus* cereus biomass. *J. Environ. Sci.* **2011**, *23*, 108–111. [CrossRef]

61. Levard, C.; Hotze, E.M.; Lowry, G.V.; Brown, G.E., Jr. Environmental transformations of silver nanoparticles: Impact on stability and toxicity. *Environ. Sci. Technol.* **2012**, *46*, 6900–6914. [CrossRef] [PubMed]

62. Li, X.; Lenhart, J.J.; Walker, H.W. Dissolution-accompanied aggregation kinetics of silver nanoparticles. *Langmuir* **2010**, *26*, 16690–16698. [CrossRef] [PubMed]

63. Liu, J.; Hurt, R.H. Ion release kinetics and particle persistence in aqueous nano-silver colloids. *Environ. Sci. Technol.* **2010**, *44*, 2169–2175. [CrossRef] [PubMed]

64. Lombi, E.; Donner, E.; Taheri, S.; Tavakkoli, E.; Jamting, A.K.; McClure, S.; Naidu, R.; Miller, B.W.; Scheckel, K.G.; Vasilev, K. Transformation of four silver/silver chloride nanoparticles during anaerobic treatment of wastewater and post-processing of sewage sludge. *Environ. Pollut.* **2013**, *176*, 193–197. [CrossRef] [PubMed]

65. Karthikeyan, S.; Beveridge, T. Pseudomonas aeruginosa biofilms react with and precipitate toxic soluble gold. *Environ. Microbiol.* **2002**, *4*, 667–675. [CrossRef] [PubMed]

66. Hoffman, L.E.; Hendrix, J.L. Inhibition of *Thiobacillus ferrooxidans* by soluble silver. *Biotechnol. Bioeng.* **1976**, *18*, 1161–1165. [CrossRef] [PubMed]

67. Zipperian, D.; Raghavan, S. Gold and silver extraction by ammoniacal thiosulfate leaching from a rhyolite ore. *Hydrometallurgy* **1988**, *19*, 361–375. [CrossRef]

68. Lawrence, R.W.; Gunn, J.D. Biological preoxidation of pyrite gold concentrate. In *Frontier Technology in Mineral Processing*; Spisak, J.F., Jergensen, G.V., Eds.; Society of Mining Engineers of AIME: New York, NY, USA, 1985; pp. 13–17.

69. Benedetti, M.; Boulegue, J. Mechanism of gold transfer and deposition in a supergene environment. *Geochim. Cosmochim. Acta* **1991**, *55*, 1539–1547. [CrossRef]

70. Xu, Y.; Schoonen, M. The stability of thiosulfate in the presence of pyrite in low-temperature aqueous solutions. *Geochim. Cosmochim. Acta* **1995**, *59*, 4605–4622. [CrossRef]

71. Aylmore, M.G.; Muir, D.M. Thiosulfate leaching of gold—A review. *Miner. Eng.* **2001**, *14*, 135–174. [CrossRef]

72. Jeffrey, M.I. Kinetic aspects of gold and silver leaching in ammonia-thiosulphate solutions. *Hydrometallurgy* **2001**, *60*, 7–16. [CrossRef]

73. Temple, K.; Colmer, A. The autotrophic oxidation of iron by a new bacterium—*Thiobacillus ferrooxidans*. *J. Bacteriol.* **1951**, *62*, 605–611. [PubMed]

74. Lyalikova, N.N. A study of chemosynthesis in *Thiobacillus ferrooxidans*. *Mikrobiologiya* **1958**, *27*, 556–559.

75. Portal, C.C.K. The World Bank Group: Climate Change Knowledge Portal Website. Available online: http://sdwebx.worldbank.org/climateportal/index.cfm (accessed on 05 May 2017).

76. Kelley, K.; Hudson, T. Natural versus anthropogenic dispersion of metals to the environment in the Wulik River area, western Brooks Range, northern Alaska. *Geochem. Explor. Environ. Anal.* **2007**, *7*, 87–96. [CrossRef]

77. Ratte, H. Bioaccumulation and toxicity of silver compounds: A review. *Environ. Toxicol. Chem.* **1999**, *18*, 89–108. [CrossRef]

78. Bridge, G. CONTESTED TERRAIN: Mining and the Environment. *Annu. Rev. Environ. Resour.* **2004**, *29*, 205–259. [CrossRef]